Real-Time Tracking of Polymer Crystallization Dynamics in Organic Bulk Heterojunctions by Raman Microscopy

Mannanov, Artur A.; Bruevich, Vladimir V.; Feldman, Elizaveta V.; Trukhanov, Vasiliy A.; Pshenichnikov, Maxim S.; Paraschuk, Dmitry Yu.

Published in:
Journal of Physical Chemistry C

DOI:
10.1021/acs.jpcc.8b03136

Publication date:
2018

Real-Time Tracking of Polymer Crystallization Dynamics in Organic Bulk Heterojunctions by Raman Microscopy

Artur A. Mannanov,[†,‡] *Vladimir V. Bruevich,*[†] *Elizaveta V. Feldman,*[†] *Vasiliy A. Trukhanov,*[†] *Maxim S. Pshenichnikov**[,‡] *and Dmitry Yu. Paraschuk**[,†,§]

[†] Faculty of Physics & International Laser Center, Lomonosov Moscow State University, Leninskie Gory 1/62, Moscow 119991, Russia.

[‡] Optical Condensed Matter Physics Group, Zernike Institute for Advanced Materials, Rijksuniversiteit Groningen, Nijenborgh 4, Groningen 9747 AG, the Netherlands.

[§] Enikolopov Institute of Synthetic Polymeric Materials, Russian Academy of Science, Profsoyuznaya 70, Moscow 117393, Russia.

ABSTRACT

State-of-the-art organic photovoltaic active layers typically undergo post-treatment such as thermal or solvent vapor annealing to increase their performance by tuning the bulk heterojunction morphology. The molecular crystallinity is one of the key factors that determine the morphology. Real-time tracking of the crystallinity during the post-treatment is strongly desired for understanding the physics of the crystallization process and for optimizing the post treatment

protocol. Here, we report on cold crystallization dynamics of the polymer in the temperature range of 50–150 °C in polymer:fullerene blends based on poly(3-hexylthiophene) with various fullerene-based acceptors (C_{60}, $PC_{61}BM$, $PC_{71}BM$, $bisPC_{61}BM$, HBIM, AIM8, and IrC_{60}) in real-time by Raman microscopy. We also reveal how different solvents, fullerene acceptors, and temperatures affect cold crystallization during thermal annealing. We further demonstrate a correlation between the fullerene derivative weight and the polymer crystallinity for the as-cast films, and also a correlation of the polymer crystallinity before and after annealing. Our findings are essential for developing efficient strategies of morphology optimization in emerging organic photovoltaic devices with the real-time Raman microscopy tracking as a valuable tool.

1. INTRODUCTION

The most efficient organic photovoltaic devices (OPDs), e.g., solar cells and photodetectors, are based on bulk heterojunctions (BHJs)[1-2] that are phase separated blends of donor and acceptor semiconductor materials.[3-6] For efficient OPDs, the organic BHJs should have a specific morphology of the donor and acceptor separated phases to provide efficient exciton dissociation, separation of free charges, and their transport to the device electrodes.[5, 7]

Polymer:fullerene blends, as the most studied BHJs, have been in the focus of research for the last two decades.[4-5, 8] In many cases, the charge generation and transport in such blends are affected by polymer crystallization,[8-9] which can be largely disturbed by fullerene acceptor molecules.[10] The polymer:fullerene blend morphology changes upon annealing have been probed by a number of experimental techniques: in-situ atomic force microscopy,[11] UV–vis spectroscopy,[12] X-ray diffraction,[9, 12] ellipsometry,[13-14] scanning electron microscopy,[15] and ultrafast spectroscopy.[16-18] For instance, as-cast poly(3-hexylthiophene) (P3HT) with [6,6]-phenyl C61 butyric acid methyl

ester ($PC_{61}BM$) blends usually show a non-optimal morphology that results in their poor photovoltaic performance, specifically in low power conversion efficiency (*PCE*).[19]

Thermal or solvent annealing are commonly used to optimize the BHJ morphology.[12, 20-22] For annealing the polymer, the following two temperatures define the operational window: the glass transition temperature T_g,[23-24] (the lower limit) and the melting temperature of the crystalline phase T_m (the upper limit). Between these two temperatures the polymer chains acquire mobility, partially crystallize and hence become more ordered — the process known as cold crystallization (CC) .[25-26] In the P3HT:$PC_{61}BM$ blends, CC results in an increase in the optical absorption at the longer wavelengths, the charge separation efficiency and carrier mobility; these all lead to a significant boost in the *PCE*.[19, 24, 27-28] For instance, differential scanning calorimetry (DSC) studies[29] revealed that the morphology of P3HT:$PC_{61}BM$ blend films results from a dual crystallization as the crystallization of both donor and acceptor phases is hindered by the other one during thermal annealing.

Raman microscopy possesses a unique ability to distinguish crystalline and amorphous domains in the BHJ.[30-31] This ability is based on the fact that the frequency of delocalized carbon-carbon stretching modes is changed upon crystallization due to interchain interactions. This approach was developed by Kim and coworkers[32] who demonstrated that the contributions of amorphous and quasi-crystalline polymer phases to the Raman spectra of P3HT:$PC_{61}BM$ blends can be factorized.[32-33] In particular, they showed that the shifts of the frequency of the Raman carbon-carbon band can be attributed to crystallization of the polymer phase in the blend films during annealing.[34] Here we refine the Raman method developed in Ref.[32] to track the polymer crystallinity *in real-time* during CC of the polymer phase and apply this technique to study thermal annealing in various P3HT:fullerene blends.

Apart from the commonly-used $PC_{61}BM$ acceptor, other fullerene-based acceptors are actively studied to increase the OPD performance via increase of the acceptor optical absorption, reduction of the acceptor electron affinity (to increase the operating voltage of OPD), and to optimize the donor:acceptor miscibility in blend.[35-39] Although it is known that the acceptor molecules in the BHJ disturbs the ordered polymer phase,[10] there is still a lack of understanding how strong its effect is on the polymer phase crystallinity in the BHJ with non-PCBM fullerene acceptors. This understanding is important for optimization of the post-deposition treatment protocols of such blends used as the OPD active layers.

In this paper, we report the polymer crystallization dynamics tracked by the real-time Raman microscopy technique during thermal annealing in the BHJ blends cast from different solvents and in the blends with various fullerene-based acceptors, with P3HT as an archetypical example. Casting blends from the higher boiling point solvent results in larger quasi-crystalline phase in as-cast films. We show a correlation of the polymer crystallinity before and after the cold crystallization. We also establish how different solvents, blend compositions, and temperatures induce the polymer mobility during thermal annealing. Thus, the real-time Raman microscopy technique provides an easy access to polymer crystallization dynamics of organic photovoltaic active layers during their post-processing.

2. MATERIALS AND METHODS

2.1. Materials. Regioregular P3HT (RR-P3HT) was purchased from Lumtec. The weight-average (Mw) and regioregularity are >45,000 kg/mol, >95%, respectively. Regiorandom P3HT (RRa-P3HT) was purchased from Rieke-Metals. The weight-average molecular weight (Mw) was >60,000 kg/mol. Different fullerene-based acceptors were studied (Supplementary Information,

SI, Section 1): C_{60}, $PC_{61}BM$, $PC_{71}BM$, 1-(3,5-di-tret-butyl-4-hydroxybenzyl)-3-(3-cyclopropane[1,9](C_{60}-Ih)[5,6]fullerene-3-yl)-indolin-2-one (HBIM),[40] 1-Tetradecyl-3-(3-cyclopropane[1,9](C_{60}-Ih)[5,6]fullerene-3-yl)-indolin-2-one (AIM8),[41] exohedral metallocomplex (η_2-C_{60})IrH(CO)[(+)-2,3-O-isopropylidene-2,3-dihydroxy-1,4-bis(diphenylphosphino)butane] (IrC_{60}),[42] and [6,6]-Diphenyl-C62-bis(butyric acid methyl ester) ($bisPC_{61}BM$)[43]. C_{60}, $PC_{61}BM$, $bisPC_{61}BM$ and $PC_{71}BM$ with purity of >99.5%; >99.5%; >99.5%; >99%, respectively, were purchased from Solenne BV. HBIM and AIM8 were obtained from Arbuzov Institute of Organic and Physical Chemistry (Russian Academy of Sciences) while IrC_{60} was obtained from Nesmeyanov Institute of Organoelement Compounds (Russian Academy of Sciences). Synthesis and characterization of HBIM, AIM8, and IrC_{60} were reported elsewhere.[40-42] All the materials were used without additional purification.

2.2. Thin films and devices. Solutions for active layers were prepared by dissolving P3HT and fullerene derivatives together in dichlorobenzene (DCB) at a weight ratio of 1:1 and a total concentration of 20 g/L. This ratio was chosen as optimal or close to optimal for solar cells based on P3HT and the studied fullerene derivatives[27, 40-44] For the P3HT:$PC_{61}BM$ and P3HT:$PC_{71}BM$ blends, chlorobenzene (CB) and chloroform (CF) solvents were also used. The solutions were stirred at a magnetic stirrer for 5 hours at 75 °C and then were spin-cast at 900 rpm on a glass substrate. The resulted film thicknesses measured with an atomic force microscope (NTEGRA Spectra, NT-MDT) were in the range of 80–150 nm. The same film preparation protocol but with other substrates was used for fabrication of organic solar cells; the details are described in SI, Section 2.

2.3. Raman spectra. Raman spectra were recorded using a Renishaw inVia Raman microscope (50x, NA=0.5 Nikon large working distance objective) in the confocal configuration. The

excitation laser wavelength was set at 488 nm (Ar^+ laser line). It has been shown that this (resonant) excitation wavelength provides high Raman sensitivity to P3HT crystallization.[32] The excitation beam power on the sample was 0.25 mW to ensure a linear excitation regime (SI, Section 3.1); the acquisition time of one Raman spectrum with ~1 cm^{-1} resolution was ~1 s. To avoid laser-induced changes of the sample (e.g. photodegradation and laser heating) under long-time exposure, the Raman spectra were collected by scanning over the sample area of ~ 100x100 μm^2 and then averaged (see SI, Section 4 for details). The sample temperature was controlled by a Linkam stage (THMS600) with nitrogen gas purging. Following Ref.[32], the Raman spectra were recorded and analyzed in the spectral region from 1350 to 1500 cm^{-1} containing the in-plane ring vibrations of P3HT: symmetric C=C stretch mode at 1450 cm^{-1} and C–C intraring stretch mode at 1380 cm^{-1} (assigned in Ref.[45]), which are highly sensitive to the crystallization of polymer chains in resonant Raman conditions.

2.4. Annealing protocols. Raman probing of polymer crystallization during thermal annealing was performed using two thermal annealing protocols: the fast and slow ones. In the fast protocol, annealing was performed under a constant elevated temperature to simulate common annealing protocols normally used to enhance the OPD performance.[46] The polymer:fullerene blend was first heated fast at the maximum heating rate (100 °C/min) up to a pre-set temperature (75, 90, 105, 120 °C) and then annealed at this temperature. The Raman spectra of the sample were recorded during the constant temperature phase of the experiment. This experiment was performed in real-time to obtain the crystallization rate *in situ*, i.e. during annealing. In the slow annealing protocol, the heating rate was set at a much lower value, 5 °C/min, to achieve quasi-static annealing,[34] in the temperature range of 20–170 °C.

2.5. Crystallinity definition. The polymer crystallinity was calculated by fitting the Raman spectrum of the sample by a linear combination of the "amorphous" and "crystalline" reference spectra as was proposed by Tsoi *et al.*[32](SI, Section 3.4). However, important difference of this study is that the spectral decomposition was performed in real time at the current temperature of the sample (i.e., without having it cooled before the Raman measurements). This approach required to obtain reference Raman spectra at all temperatures used (see below). Raman spectra of the annealed pristine RR-P3HT and RRa-P3HT:$PC_{61}BM$ (4:1 weight ratio to quench the polymer fluorescence) samples were used as the references for the quasi-crystalline and amorphous phases, respectively (SI, Section 3.4). RRa-P3HT does not crystallize,[47] whereas pristine RR-P3HT shows the highest degree of crystallinity. The pristine P3HT samples were prepared as described in Ref.[32] to facilitate direct comparison of the results.

The polymer crystallinity in blend films was quantified by the "index of polymer crystallinity" (*IPC*). The *IPC* value was defined as a fraction of the RR-P3HT spectrum in the fit to the blend film spectrum, where the fit is constructed from a superposition of both reference spectra:[32]

$$IPC(T) = P_{RR}(T) \Big/ \left(P_{RRa}(T) \times \frac{\sigma_{RR}}{\sigma_{RRa}} + P_{RR}(T) \right), \quad (1)$$

where P_{RR} and P_{RRa} are the fitting coefficients obtained as shares of the RR- and RRa-P3HT reference Raman spectra in the Raman spectrum of the blend (SI, Section 3.2); T is the temperature, $\sigma_{RR}/\sigma_{RRa} = 1.2 \pm 0.2$ is the ratio of Raman cross-sections of the reference samples (SI, Section 3.2). This ratio was obtained from Raman and Fourier-transform infrared (FTIR) absorption spectroscopy (see SI, Section 3.2). Unlike the approach based on comparing visible absorption spectra proposed in Ref.[32], the method applied here benefits from direct measurement of the chromophore density in the sample and hence should be more accurate for calculation of the

relative Raman cross-sections. *IPC*=1 corresponds to the annealed pristine RR-P3HT film, while *IPC*=0 corresponds to the amorphous polymer.

The Raman spectra of conjugated polymers depend on temperature (Figure S3a).[33, 48-49] Therefore, we measured the reference Raman spectra at all temperatures with a 1°C step and used the corresponding spectra for calculation of the *IPC* according to Equation 1. Note that the ratio of Raman cross-sections of the reference samples does not show any temperature dependence (Figure S3b).

3. RESULTS AND DISCUSSION

3.1. Real-time tracking of polymer crystallinity. Figure 1 shows polymer crystallization dynamics of P3HT:$PC_{61}BM$ and P3HT:$PC_{71}BM$ films for different annealing temperatures for the fast annealing protocol. At high temperatures (105, 120 °C), the *IPC* reaches 90% of its final value faster than in 5 min and then levels off. At low temperatures (75, 90 °C), the *IPC* dynamics exhibit different behavior: the initial crystallization rate is significantly lower, which is assigned to lower mobility of polymer chains so that the *IPC* does not reach the maximum achieved at higher temperatures. Note that *IPC*=1 does not imply that all RR-P3HT is in the crystalline state but only the fraction that can crystallize; the share of this fraction was estimated as ~10% from the DSC data.[50]

As follows from Figure 1, the higher annealing temperature results in faster *IPC* rising at the initial annealing stage for both PCBMs. However, the polymer crystallization dynamics are somewhat different: the *IPC* rising amplitude during the first 2 minutes is lower for $PC_{61}BM$ (panel a) than for $PC_{71}BM$ (panel b), i.e. from ~0.43 to ~0.65 *vs*. from ~0.49 to ~0.8. This difference is

explained by the effect of $PC_{61}BM$ and $PC_{71}BM$ on the polymer packing and will be discussed in detail in Section 3.3.

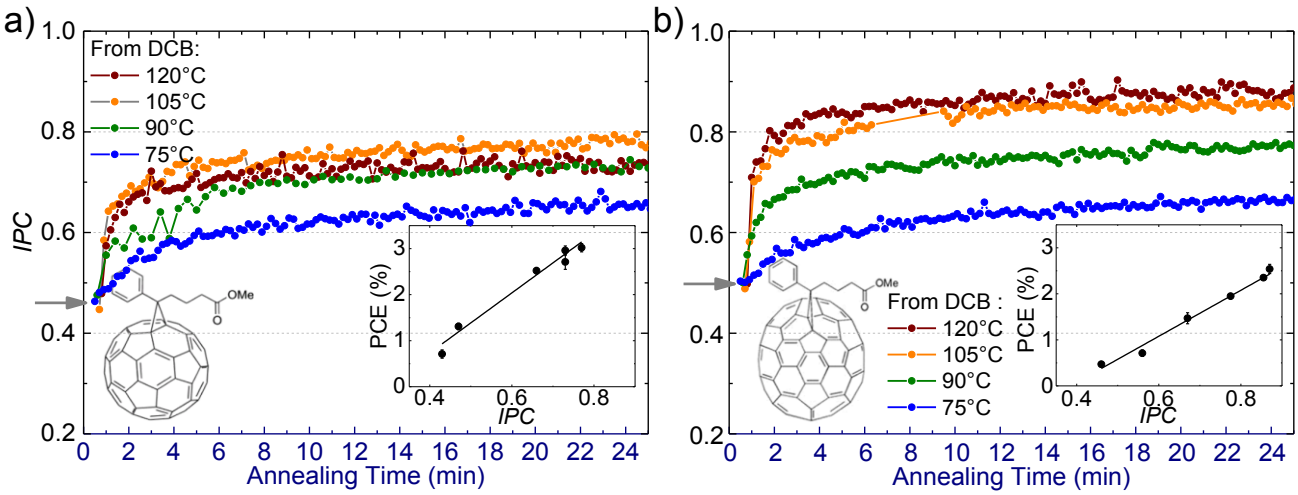

Figure 1. *IPC* dynamics in P3HT:$PC_{61}BM$ (a) and P3HT:$PC_{71}BM$ (b) blend films prepared from dichlorobenzene (DCB) for the fast annealing protocol (heating rate of 100 °C/min) at the following annealing temperatures: 75 (blue), 90 (olive), 105 (orange), 120 °C (wine). The arrows indicate the *IPC* values for the as-cast P3HT:$PC_{61}BM$ (~0.43) and P3HT:$PC_{71}BM$ (~0.49) blend films, respectively. At the initial stage of the heating process (0-1 minute), the sample temperature is not reliably established. The insets show the *PCE vs.* the final *IPC* in P3HT:$PC_{61}BM$ (a) and P3HT:$PC_{71}BM$ (b) solar cells. The lines in insets are linear fits.

The OPD performance based on P3HT:$PC_{61}BM$ blend depends strongly on the polymer crystallinity.[28, 51] Polymer crystallization results in the higher external quantum efficiency of the OPD and in the red shift of the absorption spectrum, which altogether lead to a significant *PCE* increase.[28] To investigate the effect of crystallinity on the *PCE*, the photovoltaic performance of the solar cell samples was examined (SI, Section 5). The *PCE* showed excellent correlation with the *IPC* for both P3HT:$PC_{61}BM$ and P3HT:$PC_{71}BM$ blends (Figure 1, insets).

Thermal annealing optimizes the BHJ morphology by increasing the crystallinity of the conjugated polymer chains in the active layer. This increases charge mobility and reduces the energy of the lowest electronic states thereby broadening the absorption spectrum. All this leads to an increase in the short-circuit current and the *PCE*,[52] which is fully consistent with our results. Moreover, the obtained correlation between the *IPC* and the *PCE* is in line with the previous studies probing the blend morphology and photovoltaic performance. Direct structural studies on P3HT:$PC_{61}BM$ and P3HT:$PC_{71}BM$ blends indicate that thermal annealing improves the polymer crystallinity resulting in the *PCE* increase.[36, 53-54] Furthermore, such a directly measured morphological parameter as the crystal domain purity, which is closely related to the *IPC*, clearly correlates with the *PCE* for a wide range of OPD including high-efficiency solar cells.[55]

3.2. Solvent effect. To unravel the polymer crystallization dynamics that lag behind the standard post-deposition annealing protocol, an annealing protocol with significantly slower (quasistatic) temperature increase is required. As was established previously for the P3HT:$PC_{61}BM$ blends,[34] dynamics of the C=C Raman band shift of P3HT during annealing was similar for the heating rates of 5 and 10 °C/min, indicating a quasistatic process. Therefore, for the slow annealing protocol, we chose a heating rate of 5 °C/min (Section 2), which allowed us to quantitatively describe the impact of solvent and various fullerene derivatives (Section 3.3) on the polymer crystallization.

Figure 2 shows *IPC* dynamics at the slow annealing protocol for P3HT:$PC_{61}BM$ and P3HT:$PC_{71}BM$ blend films prepared from different solvents. The data in both panels are subdivided into three areas: no evident *IPC* change at temperature below ~50°C; efficient polymer crystallization with a steep *IPC* increase in the range of 50–110°C; *IPC* levelling off at temperatures above ~110°C. According to the DSC data in Ref.[29], the glass transition temperature,

T_g, in P3HT:$PC_{61}BM$ 1:1 blends is about 50°C; therefore, T_g is well correlated with the beginning of the efficient annealing (*IPC* increase).

Annealing significantly increases the *IPC* of the P3HT:$PC_{61}BM$ blend cast from CB, from 0.31±0.04 to 0.74±0.04. The *IPC* values before and after annealing are similar to those reported in Ref.[32]: 0.42 to 0.94 (annealed at 140°C for 30 min), respectively (the *IPC* are recalculated from the crystalline molar fraction reported in Ref.[32]). The difference in the *IPC* most probably originates from different approaches to evaluate the σ_{RR}/σ_{RRa} ratio, which in Ref.[32] was reported as 0.6 (see Supporting Information in Ref.[32]). Using this value, we would obtain the *IPC* ranging from 0.45±0.04 to 0.88±0.04 before and after annealing, respectively, which is in better agreement with the values in Ref.[32]

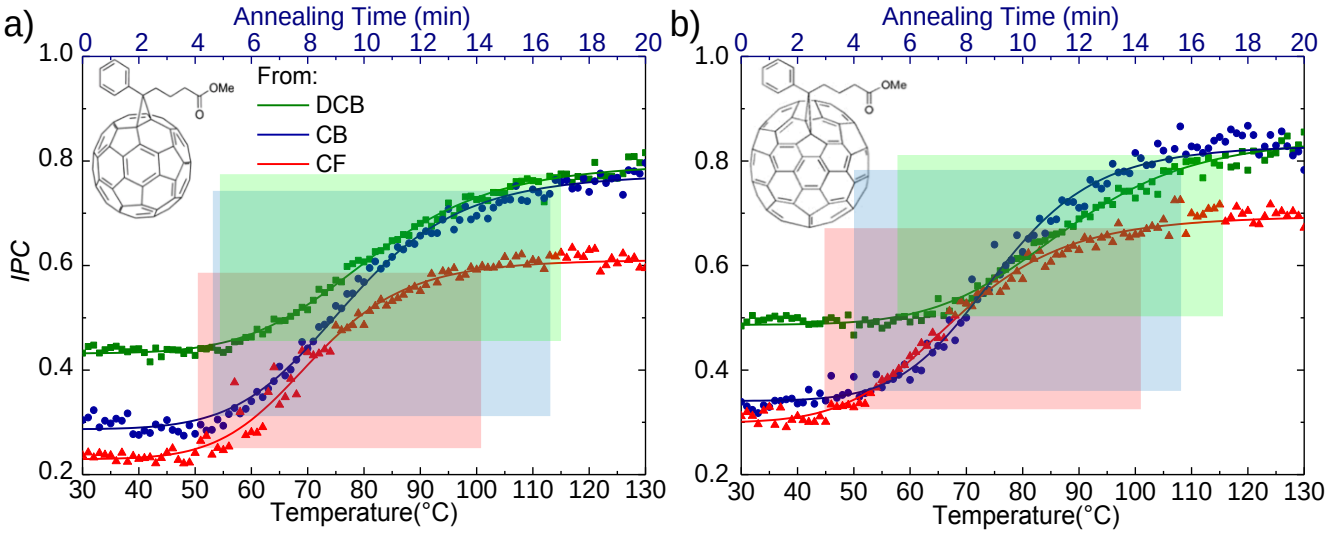

Figure 2. Real-time *IPC* dynamics at the slow (5 °C/min) annealing protocol as a function of the annealing temperature (at the bottom) and of the annealing time (at the top) for P3HT:$PC_{61}BM$ (a) and P3HT:$PC_{71}BM$ (b) blends films prepared from DCB (olive), CB (navy) and CF (red). The coordinates of the rectangles corners represent the parameters T_{CC}^{min}, T_{CC}^{max}, IPC_I, and IPC_F calculated from the curves and introduced further in Section 3.2 (for the list of the parameters, see SI, Table S2).

Figure 3 shows a schematic representation of the observed crystallization behavior of a polymer:fullerene blend at quasi-equilibrium heating (i.e., slow annealing protocol). The crystallization dynamics represented by the black curve is similar to the measured *IPC* dynamics for the P3HT:$PC_{61}BM$ blend film shown in SI, Figure S12a. According to the cold crystallization (CC) theory,[25] CC occurs above the glass transition temperature at which the amorphous phase in a polymer system can acquire mobility. In the temperature range between T_g and T_m, i.e., during the CC process, the polymer chains from the amorphous phase of the blend tend to crystallize. The polymer crystallization dynamics are irreversible in the temperature range of 50–110 °C in Figure

2 (Figure S11). This temperature range is very similar to that reported for the P3HT:$PC_{61}BM$ blend by Demir *et al*.[23], who obtained T_g = 36 °C and the CC temperature region of ~70–150 °C from the rapid-scanning DSC. In our experiments, CC occurs at somewhat lower temperatures in the range 50–110 °C. The apparent difference in the CC temperatures can be assigned to different rates at which the sample was heated.[24] In the present experiments, the heating rate was a factor of 100 slower than in the rapid-scanning DSC so that the slow annealing protocol used herein is much closer to the thermodynamic equilibrium in the blend. Another reason of the mentioned difference could be assigned to the fact that the CC temperature depends on the film thickness.[56]

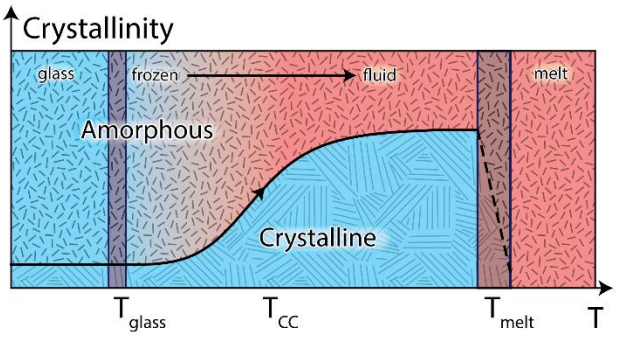

Figure 3. A schematic showing polymer crystallization from the amorphous phase as observed during slow annealing of a polymer:fullerene blend. T_g is the glass transition temperature, T_{CC} is a temperature at which the cold crystallization operates, T_m is the melting point of the semicrystalline polymer phase.

The real-time Raman microscopy technique allowed us to identify and quantify polymer crystallization in the form of temperature dependence similar to that recorded in a DSC scan. Indeed, the slow heating protocol is similar to the one routinely used in DSC. However, in contrast to DSC, the Raman technique benefits from chemical selectivity of the Raman spectrum.

Therefore, the *IPC* curves report crystallization dynamics of the polymer chains in the blend, while the DSC curves encompass features of all components in the blend including, e.g., fullerene crystallization/melting.[14] Moreover, the real-time Raman microscopy technique can be applied directly to the OPD active layer at standard OPD post-treatment conditions — this is important as T_g and the CC temperature range depend on the film thickness.[24, 56] Finally, the data collection on thin films needs a few μg of material (i.e., the amount needed for film preparation), whereas DSC usually requires special non-equilibrium conditions and several mg of material.[23, 29]

To quantify the characteristic parameters of the blend film under annealing, we define the following quantities: (1) the *IPC* of the as-cast blend film, IPC_{ac}, that is an average value of the *IPC* below 50 °C; (2) *IPC* of the annealed blend film, IPC_{an}, that is an average value of the *IPC* within a 10-degrees window around the *IPC* maximum; (3) the initial *IPC* value which is provisionally defined as the latest value above the 5% uncertainty margin of the IPC_{ac} value: $IPC_I = IPC_{ac} + (IPC_{an} - IPC_{ac})\cdot 0.05$, and a temperature corresponding to the initial *IPC*, T_{CC}^{min}, at which CC starts; (4) a temperature at which CC ends, T_{CC}^{max}, corresponding to the final *IPC*, $IPC_I = IPC_{ac} + (IPC_{an} - IPC_{ac})\cdot 0.95$. This temperature corresponds to the upper limit of CC: all the polymer chains that could crystallize have been crystallized. These four parameters are presented in Figure 2 as the coordinates of the rectangles corners (the parameter values are presented in Table S2). As follows from Figure 1, the *IPC* values before and after annealing are higher for $PC_{71}BM$, while Figure 2 demonstrates that the *IPC* in the P3HT:$PC_{71}BM$ blend is always higher than that in the P3HT:$PC_{61}BM$ blend. The difference is assigned to the larger molecule size of $PC_{71}BM$, which impedes mixing the fullerene derivative with the polymer chains and, therefore, less perturbs the polymer phase crystallinity.

As follows from Figure 2, the initial *IPC* values depend on the type of the solvent. Increasing the solvent boiling temperature in series of CF, CB, DCB (boiling temperatures are 61, 131, and 181°C, respectively) increases the solidification time of the liquid spin-cast films, which is determined by the solvent evaporation time, and results in longer time available for mobility of the polymer chains. This mobility fosters the initial crystallization during the film solidification and results in a clear correlation between the IPC_I and the solvent boiling temperature (Table S2). Note that P3HT solubilities are very close in CF, CB, DCB (14–16 g/L), whereas $PC_{61}BM$ solubilities in these solvents are different (29, 60 and 42 g/L, respectively)[57] and do not correlate with the *IPC* (Figure 2a). This could be explained by the fact that the acceptor solubility largely affects the aggregated acceptor phase but not the mixed polymer:fullerene phase and hence the *IPC*.

Figure 2 indicates that the higher boiling solvent DCB as compared to CF results in increase of the CC temperature range (the horizontal size of the rectangles) from 50–100°C to 55–115 °C and from 45–100°C to 60–120 °C for P3HT:$PC_{61}BM$ and P3HT:$PC_{71}BM$, respectively. However, the CB-cast films show the same IPC_F as those prepared from DCB. Meanwhile, the CF-cast film exhibits the lowest *IPC* that does not achieve the maximum after annealing as was observed for the other solvents. Even though the initial *IPC* of the CF-cast and CB-cast films are very close, the *IPC* in the annealed CF-cast film is significantly lower (Figure 2). This indicates that the maximal *IPC* value critically depends on the solvent type, and the fullerene acceptor solubility[58] might be an essential factor. Therefore, the particular solvent used for blend preparation can increase both IPC_I and IPC_F. However, casting blends from some solvents (e.g., CF) might negatively affect the polymer phase crystallinity not allowing the highest *IPC* value even after thermal annealing of the

blend films. As the films prepared from DCB showed the highest crystallinity, we decided to choose DCB as a solvent for the further study of blends of P3HT with different fullerene acceptors.

3.3. Various fullerene-based acceptors. In the Raman technique, the *IPC* exclusively accounts for the properties of the polymer (donor) component in BHJ. As the acceptor component could affect both amorphous and crystalline phases of the blend, we studied how various fullerene derivatives influence the polymer crystallization dynamics during annealing.

Figure 4 shows slow annealing dynamics for P3HT:fullerene 1:1 blends spin-cast from DCB. All the blends demonstrate the three consecutive annealing phases similar to P3HT:fullerene blends (Figure 2; for *IPC* dynamics of C_{60} with all three annealing phases see Figure S12b).

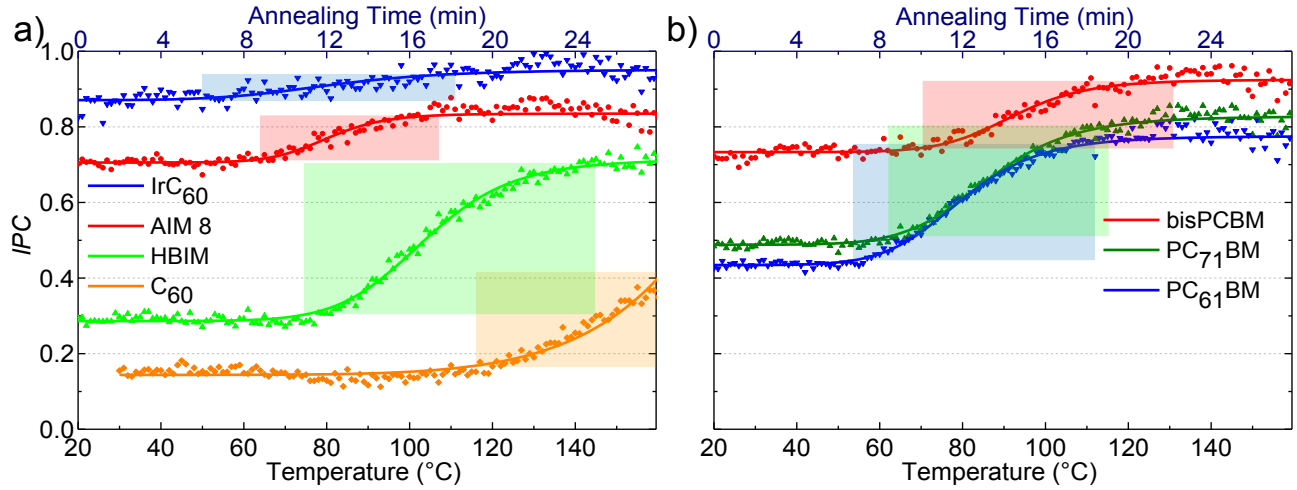

Figure 4. *IPC* for blend films of P3HT with various fullerene derivatives (in panel a: IrC_{60}, AIM8, HBIM and C_{60}; in panel b: bis$PC_{61}BM$, $PC_{71}BM$ and $PC_{61}BM$) as a function of the annealing temperature/time. The coordinates of the rectangles corners represent T_{CC}^{min}, T_{CC}^{max}, IPC_I, and IPC_F parameters calculated from the curves; for the list of the parameters see Table S2.

Both initial and final *IPC*s vary significantly for the different fullerene derivatives. While IrC_{60} and AIM8 do not reduce much the polymer crystallinity (IPC_I = 0.88 and 0.71, respectively), C_{60}

makes P3HT nearly amorphous (IPC_I = 0.17). Furthermore, Figure 4 shows that all the blends exhibit different temperatures T_{CC}^{min} at which annealing starts, from 50 to 117 °C. In contrast to the data on the P3HT:$PC_{61}BM$ blends processed from various solvents (Figure 2), the difference in T_{CC}^{min} for the various blends is much higher.

The most important parameter in the CC theory[25] is the ratio between the weights of the polymer species that can crystallize and the other blend components that are unable to contribute in the crystalline phase. In the case of P3HT:fullerene blends, this ratio highly depends on the portion of fullerene acceptor blended with the amorphous polymer phase.[23] According to the published data,[38] $PC_{61}BM$ can intercalate into the polymer crystalline phase between the nearest polymer side-chains in poly(terthiophene):$PC_{61}BM$ and poly(2-methoxy-5-(3,7-dimethyloxy)-p-phenylene vinylene):$PC_{61}BM$. Nevertheless, there is an insufficient space between the side-chains of the ordered RR-P3HT to allow the fullerene intercalation.[38] Meanwhile, all investigated fullerene derivatives are miscible with P3HT that might result in the amorphous P3HT:fullerene phase.[38, 40-43] Above T_g, the amorphous phase gains mobility allowing CC to commence, and the *IPC* starts to grow. Therefore, the CC temperature range $T_{CC}^{min} - T_{CC}^{max}$ is determined by the amorphous phase composition, namely on the polymer:fullerene weight ratio[33] and the fullerene derivative type (Table S2).

To understand whether the chemical composition of the fullerene addend affects the polymer phase crystallinity in the blend films, in **Figure 5**a we plot the IPC_I as a function of the fullerene acceptor molar volume (the IPC_I vs the fullerene weight is given in Figure S14a). The molar volumes for P3HT and C_{60}, $PC_{61}BM$, $PC_{71}BM$, bis-$PC_{61}BM$ were taken from Ref.[14] , and, for the other fullerene derivatives, were calculated as a sum of the van der Waals volumes of the fullerene cage and the corresponding addend as described in Ref.[59] (Ref.[60] for an Ir atom). Approximately

linear correlation between the IPC_I in the blend and the fullerene acceptor molar volume might be attributed to the P3HT:fullerene miscibility in the polymer amorphous phase, i.e. the less fullerene acceptor volume affects more the polymer phase leading to the lower *IPC* in as-cast blends. However, the initial *IPC* does not show any clear correlation with the fullerene acceptor solubility (Figure S13). This is in line with the data from Ref.[61], which show that the fullerene acceptor solubility albeit important, is not directly correlated with the *PCE*. Similarly to the fullerene acceptor solubility, the *PCE* generally increases with increase of the *IPC* upon annealing, but this trend is not universal (Table S2).

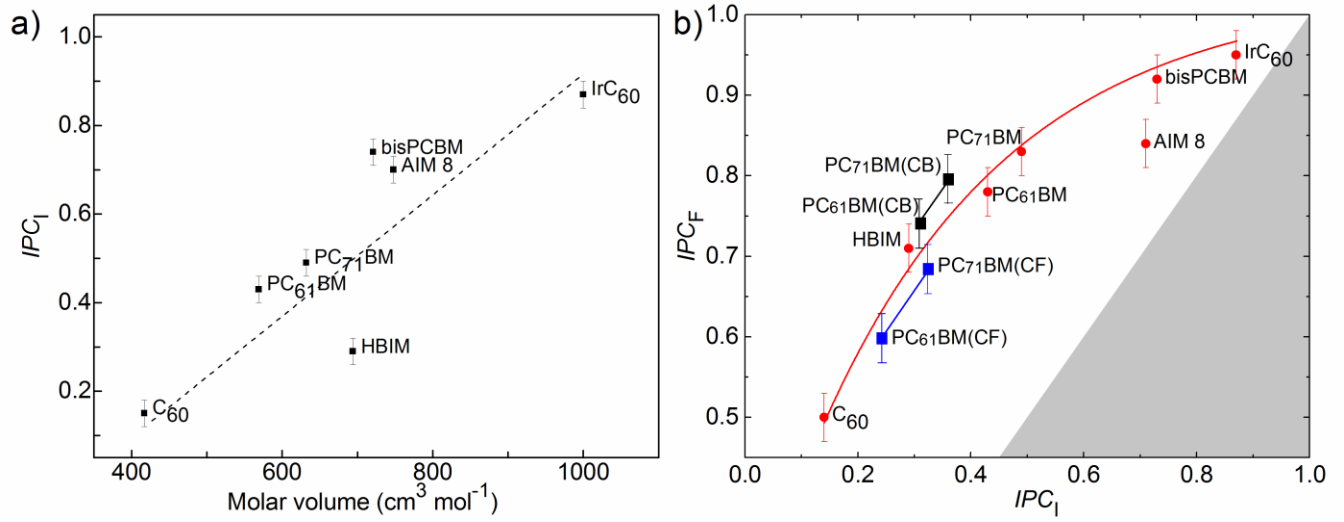

Figure 5. *IPC* charts for blends of P3HT with various fullerene derivatives. (a) Initial *IPC* (IPC_I) versus the molar volume of the fullerene derivatives. The dash line is a linear fit; (b) Final *IPC* (IPC_F) versus the initial *IPC* (red symbols are for DCB, black symbols for CB and blue symbols for CF). The red and black lines are guides to the eye. The gray shaded area corresponds to decrease of the *IPC* (i.e. $IPC_F < IPC_I$) upon annealing.

Figure 5b plots the IPC_F versus the IPC_I for all P3HT:fullerene blends studied. These *IPC*s show a positive correlation indicating that the lower limit of the IPC_F is determined by its initial value (IPC_I). Note the apparent similarity between CC and solid film formation from solution (e.g., by spin-casting): the mobility of polymer chains at temperatures higher than T_g is akin to the polymer fluidity in the liquid film formed upon film casting. As a result, polymer crystallization occurs both during film drying and thermal annealing the P3HT:fullerene blends. However, the room for the increase of polymer crystallinity is limited: more the fullerene acceptor disturbs the polymer crystallinity during film drying (leading to lower IPC_I), lower the IPC_F is after post processing (Figure 5b). This trend is in line with the CC theory of polymers.[24] Note that T_{CC}^{min} does not show any clear correlation with the fullerene acceptor volume nor its solubility nor the IPC_I (Figure S15).

4. CONCLUSIONS

In summary, we have demonstrated Raman microscopy to be a powerful tool to probe polymer cold crystallization dynamics in real time during thermal annealing. The cold crystallization of polymer chains is shown to operate within the temperature range of 50–150 °C in various P3HT:fullerene blends. The *IPC*s of P3HT:$PC_{61}BM$ and P3HT:$PC_{71}BM$ annealed blends show excellent correlation with the power conversion efficiency of organic solar cells based on the blends.

The refined Raman microscopy technique has allowed us to monitor the dynamics of cold crystallization of P3HT:fullerene blend films in real-time at subsecond timescales right during temperature annealing. This technique is similar to DSC but, in contrast, can be applied directly to the solar cells active layer and benefit from high chemical selectivity and spatial resolution. The

results show that the parameters important for polymer crystallization in the bulk heterojunction are the annealing temperature, solvent, and acceptor type. Specifically, casting blend from the higher boiling solvent results in larger quasi-crystalline phase in as-cast films. Furthermore, we found a correlation between the fullerene addend weight and the polymer crystallinity for as-cast films, and also a correlation of the polymer crystallinity at the start and end of the cold crystallization. The real-time Raman microscopy technique might be easily extended to *in-situ* study of cold crystallization dynamics during another popular annealing technique, solvent vapor annealing.

As Raman microscopy is chemically selective, it has the ability to clearly distinguish the donor and acceptor species in the blend and hence a high potential to probe crystallization of either donor or acceptor component in BHJs separately. From this point of view, it will be interesting to study crystallization of the acceptor component (be it a fullerene derivative[14] or another polymer or a small-molecule acceptor[62]), which could also contribute to charge photogeneration in organic solar cells.[63]

The spatial resolution of standard Raman microscopy as used herein does not suffice to probe the nanomorphology that of a key importance for the OPD performance.[64] Radical increase of the spatial resolution to directly distinguish donor/acceptor domains of a few tens of nm in size could be achieved with the tip-enhanced Raman microscopy.[65] Indirect morphology retrieving by time-resolved Raman microscopy[66] is also in the horizon similarly to the early-reported pump-probe approaches.[16-18] Thus, together with the ability of the Raman microscopy to distinguish crystalline and amorphous phases *in vivo* (as demonstrated in this paper) of the donor and acceptor components, makes it a powerful tool for optimization of the morphology in real-time, which is hardly accessible to other structural methods.

ASSOCIATED CONTENT

Supporting Information

The Supporting Information is available free of charge on the ACS Publications website. Chemical structures of the fullerene derivatives studied; fabrication of organic solar cells; tracking polymer crystallinity; excitation assisted laser annealing; correlation between the *PCE* and *IPC*; supporting data of the slow annealing protocol; IPC_I versus fullerene-based acceptor solubility. (PDF)

Corresponding Authors

*E-mail: paras@physics.msu.ru (D.Yu.P.);

*E-mail: m.s.pchenitchnikov@rug.nl (M.S.P.).

Author Contributions

VVB conceived the project; AAM participated in its further development. AAM performed the preparation of polymer:fullerene films and their Raman microscopy study. AAM and VVB developed the real-time protocol. EVF performed the Raman study under the standard annealing protocol. VAT fabricated the solar cells and evaluated their *PCE*s. DYuP and MSP supervised the development of the project. AAM, VVB, MSP, and DYuP wrote the manuscript.

ACKNOWLEDGMENTS

The authors would like to acknowledge I.P. Romanova for providing fullerene derivatives HBIM and AIM8, M.V. Tsikalova for providing fullerene complex IrC_{60}, A.A. Gromchenko for the data

on P3HT:IrC_{60} solar cells, I.V. Golovnin for the FTIR measurements, and N. Stingelin for fruitful discussions on cold crystallization.

DYP acknowledges partial support from the Aurora program (Erasmus Mundus Acton 2). MSP has received funding from the European Union's Horizon2020 research and innovation programme under Marie Sklodowska Curie grant agreement No. 722651. This work was supported by the Russian Science Foundation (project № 14-13-01380), and was done using equipment purchased under the Lomonosov Moscow State University Program of Development.

Notes

The authors declare no competing financial interest.

ABBREVIATIONS

OPD, organic photovoltaic device; CC, cold crystallization; *IPC*, index of polymer crystallinity; DCB, orthodichlorobenzene; CB, benzene; CF, chloroform; *PCE*, power conversion efficiency; P3HT, poly(3-hexylthiophene); $PC_{61/71}BM$, [6,6]-phenyl C61/71 butyric acid methyl ester; HBIM, 1-(3,5-di-tret-butyl-4-hydroxybenzyl)-3-(3-cyclopropane[1,9](C_{60}-Ih)[5,6]fullerene-3-yl)-indolin-2-one; AIM8, 1-Tetradecyl-3-(3-cyclopropane[1,9](C_{60}-Ih)[5,6]fullerene-3-yl)-indolin-2-one; IrC_{60}, exohedral metallocomplex (η_2-C_{60})IrH(CO)[(+)-2,3-O-isopropylidene-2,3-dihydroxy-1,4-bis(diphenylphosphino)butane]; bis$PC_{61}BM$, [6,6]-Diphenyl-C62-bis(butyric acid methyl ester).

REFERENCES

1. Yu, G.; Gao, J.; Hummelen, J. C.; Wudl, F.; Heeger, A. J., Polymer Photovoltaic Cells - Enhanced Efficiencies via a Network of Internal Donor-Acceptor Heterojunctions. *Science* **1995**, *270*, 1789-1791.

2. Armin, A.; Jansen-van Vuuren, R. D.; Kopidakis, N.; Burn, P. L.; Meredith, P., Narrowband Light Detection via Internal Quantum Efficiency Manipulation of Organic Photodiodes. *Nat. Commun.* **2015**, *6*, 6343-6351.

3. Hoppe, H.; Sariciftci, N. S., Morphology of Polymer/Fullerene Bulk Heterojunction Solar Cells. *J. Mater. Chem.* **2006**, *16*, 45-61.

4. Nelson, J., Polymer:Fullerene Bulk Heterojunction Solar Cells. *Mater. Today* **2011**, *14*, 462-470.

5. Veldman, D.; İpek, Ö.; Meskers, S. C. J.; Sweelssen, J.; Koetse, M. M.; Veenstra, S. C.; Kroon, J. M.; Bavel, S. S. v.; Loos, J.; Janssen, R. A. J., Compositional and Electric Field Dependence of the Dissociation of Charge Transfer Excitons in Alternating Polyfluorene Copolymer/Fullerene Blends. *J. Am. Chem. Soc.* **2008**, *130*, 7721-7735.

6. Liao, H.-C.; Ho, C.-C.; Chang, C.-Y.; Jao, M.-H.; Darling, S. B.; Su, W.-F., Additives for Morphology Control in High-Efficiency Organic Solar Cells. *Mater. Today* **2013**, *16*, 326-336.

7. Gunes, S.; Neugebauer, H.; Sariciftci, N. S., Conjugated Polymer-Based Organic Solar Cells. *Chem. Rev.* **2007**, *107*, 1324-1338.

8. Keivanidis, P. E.; Clarke, T. M.; Lilliu, S.; Agostinelli, T.; Macdonald, J. E.; Durrant, J. R.; Bradley, D. D. C.; Nelson, J., Dependence of Charge Separation Efficiency on Film Microstructure in Poly(3-Hexylthiophene-2,5-Diyl):[6,6]-Phenyl-C61 Butyric Acid Methyl Ester Blend Films. *J. Phys. Chem. Lett.* **2010**, *1*, 734-738.

9. Agostinelli, T.; Lilliu, S.; Labram, J. G.; Campoy-Quiles, M.; Hampton, M.; Pires, E.; Rawle, J.; Bikondoa, O.; Bradley, D. D. C.; Anthopoulos, T. D., et al., Real-Time Investigation of Crystallization and Phase-Segregation Dynamics in P3HT:PCBM Solar Cells During Thermal Annealing. *Adv. Funct. Mater.* **2011**, *21*, 1701-1708.

10. Collins, B. A.; Tumbleston, J. R.; Ade, H., Miscibility, Crystallinity, and Phase Development in P3HT/PCBM Solar Cells: Toward an Enlightened Understanding of Device Morphology and Stability. *J. Phys. Chem. Lett.* **2011**, *2*, 3135-3145.

11. Roige, A.; Campoy-Quiles, M.; Osso, J. O.; Alonso, M. I.; Vega, L. F.; Garriga, M., Surface Vs Bulk Phase Transitions in Semiconducting Polymer Films for OPV and OLED Applications. *Synth. Met.* **2012**, *161*, 2570-2574.

12. Chen, F.-C.; Ko, C.-J.; Wu, J.-L.; Chen, W.-C., Morphological Study of P3HT:PCBM Blend Films Prepared through Solvent Annealing for Solar Cell Applications. *Sol. Energy Mater. Sol. Cells* **2010**, *94*, 2426-2430.

13. Wang, T.; Dunbar, A. D. F.; Staniec, P. A.; Pearson, A. J.; Hopkinson, P. E.; MacDonald, J. E.; Lilliu, S.; Pizzey, C.; Terrill, N. J.; Donald, A. M., et al., The Development of Nanoscale Morphology in Polymer: Fullerene Photovoltaic Blends During Solvent Casting. *Soft Matter* **2010**, *6*, 4128-4134.

14. Leman, D.; Kelly, M. A.; Ness, S.; Engmann, S.; Herzing, A.; Snyder, C.; Ro, H. W.; Kline, R. J.; DeLongchamp, D. M.; Richter, L. J., In Situ Characterization of Polymer–Fullerene Bilayer Stability. *Macromol.* **2015**, *48*, 383-392.

15. Treat, N. D.; Brady, M. A.; Smith, G.; Toney, M. F.; Kramer, E. J.; Hawker, C. J.; Chabinyc, M. L., Interdiffusion of PCBM and P3HT Reveals Miscibility in a Photovoltaically Active Blend. *Adv. Energy Mater.* **2011**, *1*, 82-89.

16. Serbenta, A.; Kozlov, O. V.; Portale, G.; van Loosdrecht, P. H. M.; Pshenichnikov, M. S., Bulk Heterojunction Morphology of Polymer:Fullerene Blends Revealed by Ultrafast Spectroscopy. *Sci. Rep.* **2016**, *6*, 36236(11).

17. Grancini, G.; Polli, D.; Fazzi, D.; Cabanillas-Gonzalez, J.; Cerullo, G.; Lanzani, G., Transient Absorption Imaging of P3HT:PCBM Photovoltaic Blend: Evidence for Interfacial Charge Transfer State. *J. Phys. Chem. Lett.* **2011**, *2*, 1099-1105.

18. Westenhoff, S.; Howard, I. A.; Friend, R. H., Probing the Morphology and Energy Landscape of Blends of Conjugated Polymers with Sub-10 Nm Resolution. *Phys. Rev. Lett.* **2008**, *101*, 016102(4).

19. Padinger, F.; Rittberger, R. S.; Sariciftci, N. S., Effects of Postproduction Treatment on Plastic Solar Cells. *Adv. Funct. Mater.* **2003**, *13*, 85-88.

20. Sirringhaus, H.; Brown, P. J.; Friend, R. H.; Nielsen, M. M.; Bechgaard, K.; Langeveld-Voss, B. M. W.; Spiering, A. J. H.; Janssen, R. A. J.; Meijer, E. W.; Herwig, P., et al., Two-Dimensional Charge Transport in Self-Organized, High-Mobility Conjugated Polymers. *Nature* **1999**, *401*, 685-688.

21. Li, G.; Yao, Y.; Yang, H.; Shrotriya, V.; Yang, G.; Yang, Y., "Solvent Annealing" Effect in Polymer Solar Cells Based on Poly(3-Hexylthiophene) and Methanofullerenes. *Adv. Funct. Mater.* **2007**, *17*, 1636-1644.

22. Janssen, G.; Aguirre, A.; Goovaerts, E.; Vanlaeke, P.; Poortmans, J.; Manca, J., Optimization of Morphology of P3HT/PCBM Films for Organic Solar Cells: Effects of Thermal Treatments and Spin Coating Solvents. *Eur. Phys. J.: Appl. Phys.* **2007**, *37*, 287-290.

23. Demir, F.; Van den Brande, N.; Van Mele, B.; Bertho, S.; Vanderzande, D.; Manca, J.; Van Assche, G., Isothermal Crystallization of P3HT:PCBM Blends Studied by Rhc. *J. Therm. Anal. Calorim.* **2011**, *105*, 845-849.

24. Müller, C., On the Glass Transition of Polymer Semiconductors and Its Impact on Polymer Solar Cell Stability. *Chem. Mater.* **2015**, *27*, 2740-2754.

25. Wunderlich, B., Theory of Cold Crystallization of High Polymers. *J. Chem. Phys.* **1958**, *29*, 1395-1404.

26. Ke, B., Differential Thermal Analysis of High Polymers. Iv. Saturated Linear Polyesters. *J. Appl. Polym. Sci.* **1962**, *6*, 624-628.

27. Chirvase, D.; Parisi, J.; Hummelen, J. C.; Dyakonov, V., Influence of Nanomorphology on the Photovoltaic Action of Polymer–Fullerene Composites. *Nanotechnology* **2004**, *15*, 1317-1323.

28. Gluecker, M.; Foertig, A.; Dyakonov, V.; Deibel, C., Impact of Nongeminate Recombination on the Performance of Pristine and Annealed P3HT:PCBM Solar Cells. *Phys. Status Solidi RRL* **2012**, *6*, 337-339.

29. Zhao, J.; Swinnen, A.; Van Assche, G.; Manca, J.; Vanderzande, D.; Mele, B. V., Phase Diagram of P3HT/PCBM Blends and Its Implication for the Stability of Morphology. *J. Phys. Chem. B* **2009**, *113*, 1587-1591.

30. Gao, Y. Q.; Grey, J. K., Resonance Chemical Imaging of Polythiophene/Fullerene Photovoltaic Thin Films: Mapping Morphology-Dependent Aggregated and Unaggregated C=C Species. *J. Am. Chem. Soc.* **2009**, *131*, 9654-9662.

31. Gao, Y.; Martin, T. P.; Niles, E. T.; Wise, A. J.; Thomas, A. K.; Grey, J. K., Understanding Morphology-Dependent Polymer Aggregation Properties and Photocurrent

Generation in Polythiophene/Fullerene Solar Cells of Variable Compositions. *J. Phys. Chem. C* **2010**, *114*, 15121-15128.

32. Tsoi, W. C.; James, D. T.; Kim, J. S.; Nicholson, P. G.; Murphy, C. E.; Bradley, D. D. C.; Nelson, J.; Kim, J. S., The Nature of in-Plane Skeleton Raman Modes of P3HT and Their Correlation to the Degree of Molecular Order in P3HT:PCBM Blend Thin Films. *J. Am. Chem. Soc.* **2011**, *133*, 9834-9843.

33. Razzell-Hollis, J.; Limbu, S.; Kim, J.-S., Spectroscopic Investigations of Three-Phase Morphology Evolution in Polymer: Fullerene Solar Cell Blends. *J. Phys. Chem. C* **2016**, *120*, 10806-10814.

34. Razzell-Hollis, J.; Tsoi, W. C.; Kim, J.-S., Directly Probing the Molecular Order of Conjugated Polymer in OPV Blends Induced by Different Film Thicknesses, Substrates and Additives. *J. Mater. Chem. C* **2013**, *1*, 6235-6243.

35. Trukhanov, V. A.; Paraschuk, D. Y., Non-Fullerene Acceptors for Organic Solar Cells. *Polym. Sci., Ser. C* **2014**, *56*, 72-83.

36. Ma, W.; Yang, C.; Gong, X.; Lee, K.; Heeger, A. J., Thermally Stable, Efficient Polymer Solar Cells with Nanoscale Control of the Interpenetrating Network Morphology. *Adv. Funct. Mater.* **2005**, *15*, 1617-1622.

37. He, Y. J.; Li, Y. F., Fullerene Derivative Acceptors for High Performance Polymer Solar Cells. *Phys. Chem. Chem. Phys.* **2011**, *13*, 1970-1983.

38. Mayer, A. C.; Toney, M. F.; Scully, S. R.; Rivnay, J.; Brabec, C. J.; Scharber, M.; Koppe, M.; Heeney, M.; McCulloch, I.; McGehee, M. D., Bimolecular Crystals of Fullerenes in Conjugated Polymers and the Implications of Molecular Mixing for Solar Cells. *Adv. Funct. Mater.* **2009**, *19*, 1173-1179.

39. Ye, L.; Hu, H.; Ghasemi, M.; Wang, T.; Collins, B. A.; Kim, J.-H.; Jiang, K.; Carpenter, J. H.; Li, H.; Li, Z., et al., Quantitative Relations between Interaction Parameter, Miscibility and Function in Organic Solar Cells. *Nat. Mater.* **2018**, *17*, 253-260.

40. Valitov, M. I.; Romanova, I. P.; Gromchenko, A. A.; Shaikhutdinova, G. R.; Yakhvarov, D. G.; Bruevich, V. V.; Dyakov, V. A.; Sinyashin, O. G.; Paraschuk, D. Y., Indolinone-Substituted Methanofullerene—a New Acceptor for Organic Solar Cells. *Sol. Energy Mater. Sol. Cells* **2012**, *103*, 48-52.

41. Romanova, I. P.; Bogdanov, A. V.; Izdelieva, I. A.; Trukhanov, V. A.; Shaikhutdinova, G. R.; Yakhvarov, D. G.; Latypov, S. K.; Mironov, V. F.; Dyakov, V. A.; Golovnin, I. V., et al., Novel Indolin-2-One-Substituted Methanofullerenes Bearing Long N-Alkyl Chains: Synthesis and Application in Bulk-Heterojunction Solar Cells. *Beilstein J. Org. Chem.* **2014**, *10*, 1121-1128.

42. Zapunidy Sergey, A.; Martyanov Dmitry, S.; Nechvolodova Elena, M.; Tsikalova Marina, V.; Novikov Yuri, N.; Paraschuk Dmitry, Y., Approaches to Low-Bandgap Polymer Solar Cells: Using Polymer Charge-Transfer Complexes and Fullerene Metallocomplexes. *Pure Appl. Chem.* **2008**, *80*, 2151-2161.

43. Kim, C.-H.; Song, M.; Jin, S.-H.; Lee, J. W., High Open-Circuit Voltage of Organic Bulk Heterojunction Solar Cells Base on Poly(3-Hexylthiophene): Fullerene Derivatives. *Mol. Cryst. Liq. Cryst.* **2011**, *538*, 216-222.

44. Balderrama, V. S.; Estrada, M.; Viterisi, A.; Formentin, P.; Pallarés, J.; Ferré-Borrull, J.; Palomares, E.; Marsal, L. F., Correlation between P3HT Inter-Chain Structure and Jsc of P3HT:PC[70]BM Blends for Solar Cells. *Microelectron. Reliab.* **2013**, *53*, 560-564.

45. Yacoby, Y.; Ehrenfreund, E., Resonant Raman-Scattering in Conjugated Polymers. *Top. Appl. Phys.* **1991**, *68*, 73-135.

46. Inoue, K.; Ulbricht, R.; Madakasira, P. C.; Sampson, W. M.; Lee, S.; Gutierrez, J.; Ferraris, J.; Zakhidov, A. A., Temperature and Time Dependence of Heat Treatment of RR-P3HT/PCBM Solar Cell. *Synth. Met.* **2005**, *154*, 41-44.

47. Shen, X. B.; Duzhko, V. V.; Russell, T. P., A Study on the Correlation between Structure and Hole Transport in Semi-Crystalline Regioregular P3HT. *Adv. Energy Mater.* **2013**, *3*, 263-270.

48. Paraschuk, D. Y.; Arnautov, S. A.; Shchegolikhin, A. N.; Kobryanskii, V. M., Temperature Evolution of Electronic and Lattice Configurations in Highly Ordered Trans-Polyacetylene. *JETP Lett.* **1996**, *64*, 658-663.

49. Osotov, M. O.; Bruevich, V. V.; Paraschuk, D. Y., Thermal Vibrational Disorder of a Conjugated Polymer in Charge-Transfer Complex. *J. Chem. Phys.* **2009**, *131*, 094906(5).

50. Malik, S.; Nandi, A. K., Crystallization Mechanism of Regioregular Poly(3-Alkyl Thiophene)S. *J. Polym. Sci., Part B: Polym. Phys.* **2002**, *40*, 2073-2085.

51. Li, G.; Shrotriya, V.; Huang, J. S.; Yao, Y.; Moriarty, T.; Emery, K.; Yang, Y., High-Efficiency Solution Processable Polymer Photovoltaic Cells by Self-Organization of Polymer Blends. *Nat. Mater.* **2005**, *4*, 864-868.

52. Wang, T.; Pearson, A. J.; Lidzey, D. G.; Jones, R. A. L., Evolution of Structure, Optoelectronic Properties, and Device Performance of Polythiophene:Fullerene Solar Cells During Thermal Annealing. *Adv. Funct. Mater.* **2011**, *21*, 1383-1390.

53. Abu-Zahra, N.; Algazzar, M., Effect of Crystallinity on the Performance of P3HT/PC70BM/N-Dodecylthiol Polymer Solar Cells. *J. Sol. Energy Eng.* **2013**, *136*, 021023(7).

54. Chandrasekaran, N.; Gann, E.; Jain, N.; Kumar, A.; Gopinathan, S.; Sadhanala, A.; Friend, R. H.; Kumar, A.; McNeill, C. R.; Kabra, D., Correlation between Photovoltaic Performance and Interchain Ordering Induced Delocalization of Electronics States in Conjugated Polymer Blends. *ACS Appl. Mater. Interfaces* **2016**, *8*, 20243-20250.

55. Jiao, X.; Ye, L.; Ade, H., Quantitative Morphology–Performance Correlations in Organic Solar Cells: Insights from Soft X-Ray Scattering. *Adv. Energy Mater.* **2017**, *7*, 1700084.

56. Campoy-Quiles, M.; Sims, M.; Etchegoin, P. G.; Bradley, D. D. C., Thickness-Dependent Thermal Transition Temperatures in Thin Conjugated Polymer Films. *Macromol.* **2006**, *39*, 7673-7680.

57. Machui, F.; Langner, S.; Zhu, X.; Abbott, S.; Brabec, C. J., Determination of the P3HT:PCBM Solubility Parameters via a Binary Solvent Gradient Method: Impact of Solubility on the Photovoltaic Performance. *Sol. Energy Mater. Sol. Cells* **2012**, *100*, 138-146.

58. Wang, C. I.; Hua, C. C., Solubility of C60 and PCBM in Organic Solvents. *J. Phys. Chem. B* **2015**, *119*, 14496-14504.

59. Bondi, A., Van Der Waals Volumes and Radii. *J. Phys. Chem.* **1964**, *68*, 441-451.

60. Ping, M.; Xiubin, L.; Yuankai, W., A Formula for Calculating Atomic Radii of Metals. *J. Chem. Educ.* **1990**, *67*, 218.

61. Troshin, P. A.; Hoppe, H.; Renz, J.; Egginger, M.; Mayorova, J. Y.; Goryachev, A. E.; Peregudov, A. S.; Lyubovskaya, R. N.; Gobsch, G.; Sariciftci, N. S., et al., Material Solubility-Photovoltaic Performance Relationship in the Design of Novel Fullerene Derivatives for Bulk Heterojunction Solar Cells. *Adv. Funct. Mater.* **2009**, *19*, 779-788.

62. Cheng, P.; Li, G.; Zhan, X.; Yang, Y., Next-Generation Organic Photovoltaics Based on Non-Fullerene Acceptors. *Nat. Photonics* **2018**, *12*, 131-142.

63. Jamieson, F. C.; Domingo, E. B.; McCarthy-Ward, T.; Heeney, M.; Stingelin, N.; Durrant, J. R., Fullerene Crystallisation as a Key Driver of Charge Separation in Polymer/Fullerene Bulk Heterojunction Solar Cells. *Chem. Sci.* **2012**, *3*, 485-492.

64. Noriega, R.; Rivnay, J.; Vandewal, K.; Koch, F. P. V.; Stingelin, N.; Smith, P.; Toney, M. F.; Salleo, A., A General Relationship between Disorder, Aggregation and Charge Transport in Conjugated Polymers. *Nat. Mater.* **2013**, *12*, 1038-1044.

65. Deckert-Gaudig, T.; Taguchi, A.; Kawata, S.; Deckert, V., Tip-Enhanced Raman Spectroscopy - from Early Developments to Recent Advances. *Chem. Soc. Rev.* **2017**, *46*, 4077-4110.

66. Fausti, D.; H.M. van Loosdrecht, P., Time-Resolved Raman Scattering. In *Optical Techniques for Solid-State Materials Characterization*, Prasankumar, R. P.; Taylor, A. J., Eds. 2011.

TOC Graphic

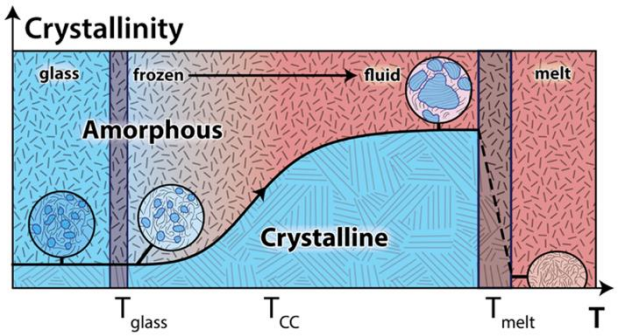
Crystallinity
glass
frozen
fluid
melt
Amorphous
Crystalline
T glass
T CC
T melt
T